Journal of Materials Chemistry B

Optical Stereolithography of Antifouling Zwitterionic Hydrogels

Journal:	*Journal of Materials Chemistry B*
Manuscript ID	TB-ART-02-2019-000278.R1
Article Type:	Paper
Date Submitted by the Author:	18-Mar-2019
Complete List of Authors:	Pan, Wenyang; Cornell University, Materials Science & Engineering Wallin, Thomas; Cornell University, Materials Science & Engineering ODENT, JEREMY; Cornell University, Materials Science & Engineering Yip, Mighten; NewYork-Presbyterian Hospital; Weill Cornell Medicine Psychiatry, Dalio Institute of Cardiovascular Imaging; Weill Cornell Medicine Psychiatry, Department of Radiology Mosadegh, Bobak; NewYork-Presbyterian Hospital; Weill Cornell Medicine Psychiatry, Dalio Institute of Cardiovascular Imaging; Weill Cornell Medicine Psychiatry, Department of Radiology Shepherd, Robert; Cornell University, Mechanical & Aerospace Engineering Giannelis, Emmanuel; Cornell University, Materials Science & Engineering

Optical Stereolithography of Antifouling Zwitterionic Hydrogels

Wenyang Pan[1], Thomas J. Wallin[1], Jérémy Odent[1], Mighten C. Yip[2,3], Bobak Mosadegh[2,3],

*Robert F. Shepherd[4], Emmanuel P. Giannelis[1]**

[1]Materials Science & Engineering, Cornell University, Ithaca, NY 14853

[2]Dalio Institute of Cardiovascular Imaging, New York-Presbyterian Hospital and Weill Cornell Medicine, New York, NY, 10065.

[3]Department of Radiology, Weill Cornell Medicine, New York, NY, 10065.

[4]Sibley School of Mechanical & Aerospace Engineering, Cornell University, Ithaca, NY 14853.

Abstract:

This paper reports the rapid 3D printing of tough (toughness, U_T, up to 141.6 kJ m^{-3}), highly solvated (ϕ^{water}~60 v/o), and antifouling hybrid hydrogels for potential uses in biomedical, smart materials, and sensor applications, using a zwitterionic photochemistry compatible with stereolithography (SLA). A Design of Experiments (DOE) framework was used for systematically investigating the multivariate photochemistry for SLA generally and, specifically, to determine an aqueous SLA system with additional zwitterionic acrylate, which significantly increases the gelation rate, and the resilience of the resulting hybrid hydrogels relative to an equivalent non-ionic polyacrylamide hydrogel. Specifically, the resulting zwitterionic hybrid hydrogels (Z-gels) can be tuned over a large range of ultimate strains, *ca.* $0.5<\gamma_{ult}<5.0$, and elastic moduli, *ca.* $10<E<1000$ kPa, while also demonstrating high resilience under cyclic, tensile loading. Importantly, unlike traditional chemistry, increasing the elastic modulus of the Z-gels does not necessarily reduce the ultimate strain. Moreover, the Z-gels can be rapidly printed using a desktop commercial SLA 3D printer, with relatively low photoirradiation dosages of visible light (135 to 675 mJ cm^{-2} per 50-100 μm layer). Compared with counterpart polyacrylamide hydrogels, Z-gels have greater antifouling property and represented 58.2 % less absorption of bovine serum albumin.

Introduction

Hydrogels are percolated networks of hydrophilic polymers, and are of considerable interests as smart biomaterials. These systems can possess mechanical properties similar to natural tissues (with elastic modulus ranging from 1 kPa <E< 10 MPa) and, in the case of acrylates (for example), are easily tuned for specific chemical responses (e.g., swelling with physiological solutions necessary to promote cellular activity and growth) [1, 2]. It is common to find these networks molded for numerous biomedical applications including DNA electrophoresis, drug delivery implants, biocompatible sensors and engineered tissues [3]. Many next generation uses of these materials (as actuator, smart stimuli-responsive materials, or implantable scaffolds) require more complex, three-dimensional patterning than molding affords [4, 5], while still maintaining properties that allow the hydrogels to be 3D printed.

Projection stereolithography (p-SLA) is a 3D printing strategy that selectively creates a desired structure layer-by-layer out of a liquid pre-gel solution under exposure to patterned light (Fig. 1A). Unlike other 3D printing approaches, the spatial localization of the photopolymerization during SLA allows one to construct complex large-scale (tens of cm) objects of near arbitrary geometry with micron-scale resolution [6]. Recently, high throughput SLA via Continuous Liquid Interface Production (CLIP) has further expanded the application space to include mass production by drastically reducing fabrication times [7]. The mechanical simplicity of p-SLA and CLIP (i.e., one degree of freedom motion control), as well as the vat polymerization process it uses, makes this technique highly amenable to innovative photochemistry for functional materials.

In general, an ideal p-SLA compatible material is a low apparent viscosity (normally, μ_{app} < 5 Pa·s) liquid that flows quickly to form a new layer (patterning time < 15 s per layer) as it

photopolymerizes into a self-supporting solid structure [8, 9]. Many hydrogels printed via SLA use concentrated solutions of low M_w acrylates, e.g. poly (ethylene glycol) diacrylate or acrylamide monomer (AAm), that quickly extend and crosslink during photo-exposure. The small mesh sizes of these gel networks, however, yield relatively brittle materials and narrow the utility of the resulting parts to prototype demonstrations [10]. Applications such as tissue engineering, actuation, or chemical sensing, for example, would benefit from resilient, tough, and highly swellable hydrogels (i.e., tunable crosslink density and polymer concentrations) [11, 12]. While less time-sensitive casting and molding processes allow for low crosslink density in polymer gels (e.g., improving the ultimate strain, γ_{ult}, of the material), most SLA printers do not produce large enough photoirradiation dosages and thus require prohibitively long exposure times for low crosslink density networks to gel.

One major strategy to improve the mechanical properties of the printed hydrogels is the use of double-network (DN) chemistries, which are typically composed of one heavily crosslinked (high E) polymer network and another interpenetrating, but lightly crosslinked (high γ_{ult}) network [13, 14]. Previously, research efforts on cast polyacrylamide (PAAm) DN hydrogels yielded high toughness and great ductility [13, 14]. The improved toughness results from the energy dissipation of the highly crosslinked network fragmenting into small clusters during mechanical deformation, while the flexible, loosely crosslinked network elastically deforms and uses the broken micro-scale primary network as physical entanglements [13]. Unfortunately, this DN loses high toughness after the first loading cycle as the covalent crosslinks undergo permanent damages. The lack of recoverable mechanical performance restricts these DN hydrogels from use in practical devices that require repeated loadings [15]. Therefore, many attempts have sought to replace permanent sacrificial crosslinks with dynamic, recoverable

bonds [15-20]. Among the potential alternatives, ionic bonds offer significant promise owing to their rapid energy dissipation during Coulombic bond breaking-reforming [21, 22]. For example, Sun et al. reported a highly stretchable and tough alginate-PAAm hydrogel, which relies on the formation and breaking of calcium-alginate ionic clusters [23, 24]. This "unzipping" of the multivalent ionic clusters, instead of the rupture of covalent bonds, leads to a slow recovery of mechanical properties from the first deformation [25].

Here we introduce a new approach based on additional zwitterionic comonomer to PAAm network for providing dynamic ionic bonds as the secondary network along the polymer backbone. This hybrid resin uses water-soluble riboflavin and triethanolamine (TEOHA) as the photoinitiator and coinitiator, respectively (Fig. 1B) [26, 27]. Unlike the traditional DN hydrogels, this reaction requires only one step and allows for more direct and rapid SLA 3D printing. Zwitterionic acrylates possess both negative and positive charges, which endow the materials with significant electrostatic attraction to water, low coefficient of friction, and extremely low bio-absorption that have resulted in their use as biocompatible surfaces or coatings, lubricants, and antifouling implantable devices [28-32]. For example, implants made of zwitterionic hydrogels significantly reduce foreign-body reactions in mice [33, 34]. Compared with biocompatible poly(ethylene glycol) derivatives which are easily oxidized, zwitterionic materials impart higher resistance to oxidation and provide opportunities for long-term applications [35]. Additionally, riboflavin and TEOHA, unlike commercial photoinitiators such as Irgacure®, have much lower cytotoxicity, initiate over lower energy visible wavelengths, and possess better solubility in aqueous solutions [36]. Due to these factors, we evaluated the potential of this hybrid hydrogel system (referred to as Z-gel henceforth) for biomedical

applications by measuring their absorption of bovine serum albumin (BSA) as a metric for their antifouling properties.

With numerous interdependent variables involved in the structure-process-property relationship of photopolymerized hydrogels (e.g., monomer concentration, crosslink density, and photoirradiation dosage), we applied the design of experiments (DOE) methodology to quantify the influence of these factors on the patterning efficiency and the physicochemical properties of the resulting hydrogels. To provide quantitative measures for DOE, we used photo-rheometer and photo-Differential Scanning Calorimetry (photo-DSC) to obtain *in situ* gelation, polymerization and rheological evolution data. Using the results of this DOE process, we identified appropriate precursor materials for the rapid 3D fabrication of resilient, tough and antifouling Z-gels.

Results and Discussion

Photopolymerizable Z-gels contain intrinsic dynamic ionic bonds that improve toughness and resilience

For the rapid gelation of hydrogels with high tensile strength and large elastic strains, we copolymerize acrylamide (AAm) and zwitterionic acrylate, [2-(methacryloyloxy)ethyl] dimethyl-(3-sulfopropyl) ammonium hydroxide (MEDSAH), using *N,N*'-methylene bis (acrylamide) (MBA) as the multi-functional crosslinker (Fig. 1B). MEDSAH, due to its strongly ionizable sulfonate groups, easily dissolves within a wide pH range in aqueous solution [37, 38]. Ionic interactions, which arise between the anionic sulfonate groups and cationic quaternary amine groups from neighboring zwitterionic moieties, produce additional electrostatic crosslinks that lead to resilient and tough hydrogels.

In the preliminary experiments, we have applied different MEDSAH to AAm weight ratios (from 0 to 100 %) in the hybrid resins. Owing to the acidity of MEDSAH, more than 50 wt% MEDSAH led to acidic resins, in which more TEOHA needs to be used to maintain the reins in the reasonable pH range (neutral to slightly basic) for the riboflavin photochemistry. While using the same contents of riboflavin and TEOHA, gelation performance peaked when the hybrid resin contained ~50 wt% MEDSAH (equivalent to ~20 % in molar ratio). In addition, MEDSAH has much higher molecular weight than AAm (279 Da vs. 71 Da). During the photo-polymerization, bulky pendant groups (e.g., large zwitterionic moieties from MEDSAH) might sterically hinder the formation of high M_w polymers. Similar results have been reported previously [39]. In GPC measurements, we did observe higher molecular weight (Mw: 881.7 kDa vs. 391.3 kDa) of non-crosslinked photopolymerized PAAm than that of non-crosslinked Z-gel (monomers ratio ~50:50, wt/wt).

Therefore, to identify an appropriate SLA material, we reduced the number of potential experiments to a tractable amount by fixing the weight ratio of AAm to MEDSAH to 50:50 (molar ratio ~80:20) in this study. This ratio is similar to that of previously published ionomers, which normally have up to 15-20 mol% ionic species [40].

Based on photo-rheological results, introducing MEDSAH into AAm solutions significantly improves the gelation rate, which is indicated by the more rapid rise of the G′ (Fig. 2A, Fig. S1). To minimize the reduction of the elastic strain regime from the addition of covalent crosslinker, we kept the MBA content low (C_{MBA} ~0.011M) in both pre-gel solutions. Additionally, according to the multiple combinations of formulation composition and photoirradiation dosage based on DOE, the Z-gels achieve significantly higher G′ and G″ over the counterpart PAAm hydrogels (270 and 1,361 times higher, respectively). These observations indicate that adding the dynamic ionic network significantly improves the gelling rate of the hydrogels, which is critical for SLA fabrication.

Unlike conventional SLA solutions, in Z-gels formulations, the rapid gelation and increase in G′ does not correspond to a reduction in extensibility. To quantify our control over the mechanical properties of the Z-gels, we performed tensile tests (Fig. 2B). The results show the Z-gels can be tuned to a wide range of elastic moduli ($10<E<1000$ kPa) and high ultimate strains ($0.5 < \gamma_{ult} < 5.0$), depending on the composition and photoirradiation dosage (Γ). By comparison, the same photoirradiation dosages applied to counterpart AAm solutions yield hydrogels that are too weak to load onto the tensile testing machine (Fig. 2C). This difference in tensile mechanical performance is easily inferred from the photo-rheological measurements (Fig. 2A).

Another major advantage of ionic crosslinks over the sacrificial covalent crosslinks is the ability to provide significant recoverable elastic deformation under tension. In our study, the Z-gel survived numerous loadings (N=100, strain γ=1) demonstrating high resilience and toughness. It is worth noting that the stress-strain curves shift upwards in later cycles, due to the incorporation of residual stresses resulting from evaporative water loss during the 12 hours of measurement (Fig. 2D). We attribute this outstanding resilience to the dynamic electrostatic interactions that dissipate the deformation energy primarily through the relaxation of the polymer chains via spontaneous breaking-reattaching of ionic bonds between adjacent sulfonate-quaternary amine groups. Previous research by Guo et al. and Long et al. also proved that stress relaxation in recoverable DN hydrogels is dominated by the breaking and reattaching of reversible dynamic bonds, instead of the permanent rupture of covalent crosslinks [41, 42].

In addition to the mechanical testing and oscillatory rheology measurements, we evaluated the thermal stability of the as prepared hydrogels using oscillatory rheology over a temperature sweep between 4 and 70°C (Fig. 2E). The evolution of moduli (G′ and G″) from this heating-cooling cycle showed that both the Z-gel and the counterpart PAAm hydrogel were stable over a broad range of temperature.

Our hybrid zwitterionic hydrogel system is also quite distinct from alginate-AAm ionic hydrogels, where the type and valence of exogenous cations play a critical role in the mechanical performance [43]. For example, the addition of multivalent cations (e.g., Ca^{2+} or Al^{3+}) is required for toughening alginate-AAm hydrogels, while gels supplemented by Na^{+} show only minimal improved toughness [23]. By attaching the ionic groups to the polymeric backbone, the Z-gel's ionic interactions remain largely unaffected by exogenous salts that will be encountered in physiologically relevant environments. Thus, the photopolymerization kinetics (e.g., gelation

speed and moduli) did not change when adding equivalent molar content of sodium (monovalent) or even calcium (divalent) chloride salts to the zwitterionic monomers (Fig. S2). Therefore, we attribute the enhanced moduli, ultimate strain and the rapid gelling performance shown in Z-gels to interactions among zwitterionic neighboring moieties.

DOE optimization of Z-gels for SLA 3D printing

Due to the complexity of the system, multiple factors simultaneously affect the efficiency and rate of photopolymerization, as well as the properties of the resulting hydrogels. Firstly, fine-tuning of the riboflavin and TEOHA is critical because the rate of free radical polymerization depends on their combined and relative amounts in aqueous solutions [26]. Neutral to basic conditions in the pre-gel solutions are reported to facilitate the formation of the riboflavin-TEOHA radical pairs, which then initiates the free radical polymerization [44]. Moreover, the monomer content (C_{resin}), crosslink density (C_{MBA}), and degree of polymerization, impact the mechanical properties of hydrogels. Consequently, we tailored these parameters with an eye towards increased printing speed and optimum properties of elastomeric hydrogels. With an intractable amount of chemical compositions and external variables to control, we used DOE methodology to narrow the design space and perform a thorough investigation of the SLA system.

First, we investigated the ratio and total amount of photoinitiator and coinitiator within a simplest AAm pre-gel solution containing a fixed amount of MBA, aiming to identify combinations that enable rapid photopolymerization (Table 1). We found that with different combinations of riboflavin and TEOHA, the gel point varied broadly from 25 s to 300 s when exposed to a low photoirradiation dosage (Omnicure Series 1500, photoirradiation density ~6.20 mW cm^{-2}, Lumen dynamic) (Fig. 3A). From the results, we selected 7.1 μL of 1 mg mL^{-1}

riboflavin as an efficient photoinitiator dosage and 71.4 μL of 300 mg mL^{-1} TEOHA, per gram of monomers for the rapid gelling, and maintaining the pre-gel solutions in the appropriate pH range, even with the addition of acidic MEDSAH comonomer.

After fixing the photoinitoator and sensitizer concentrations, we used multi-factorial and multi-level response surface designs in DOE to investigate the effects of monomer content, crosslink density and photoirradiation dosage on the gelation and the resulting mechanical performance (Table 2). We selected the storage modulus (G′) of the gelling network, tensile elastic modulus (E) of the resultant elastomer, and ultimate strain (γ_{ult}) as the key mechanical metrics. Unsurprisingly, the corresponding models show that higher monomer content, crosslink density, or photoirradiation dosage (represented as the exposure time) results in a stiffer but less stretchable hydrogel (Fig. 3B, C; Tables 2, S1, S2). To gain deeper insight, we used photoirradiation dosage as the tuning parameter to understand what pre-gel solution compositions could produce desirable mechanical properties at low dosages, required by fast SLA process. Choosing relatively low photoirradiation dosage ($\Gamma \sim$ 372 mJ cm^{-2}) as our objective, led to a formulation with excellent ultimate strain (γ_{ult}= 4.76, at an E ~246 kPa).

We then used DOE to investigate the swelling behavior of the Z-gels (swelling ratio, $= {W_s}/{W_0}$). While some applications benefit from hydrogel swelling (e.g., osmotic actuation) [18], other applications, e.g., implantable biomedical devices, prefer a low q. We soaked all the as-prepared Z-gels in 37°C deionized water for 48 hours until the absorbed weight plateaued. We clearly observed the inverse correlation of q versus C_{resin}, C_{MBA}, and t_{exp} (Table 2; Fig. S3), among which crosslink density (C_{MBA}) is slightly more influenced followed by the photoirradiation dosage and then C_{resin}. Among all combinations in DOE, the formulation with

C_{resin}=4.37 M, C_{MBA}=0.024 M MBA and Γ=279 mJ cm^{-2} has pretty good ultimate strain (γ_{ult}=3.81) and relatively low swelling ratio (q=1.48).

While the Z-gels we have so-far reported show tunable mechanical properties and swelling, we have used DOE to optimize t_{gel}, which we defined as when G′ >1 Pa, of AAm and zwitterionic formulations to be more compatible with rapid layer fabrication in SLA, using photo-rheological results. Consistent with expectations, we found that increasing C_{resin} or C_{MBA} decreases the photoirradiation necessary for gelation (Fig. 3D, E; Tables 3, S3, S4). For example, when C_{resin} is fixed, increased C_{MBA} leads to faster polymerization (Fig. S4A). On the other hand, with a fixed C_{MBA}, more concentrated pre-gel solutions gel more rapidly (Fig. S4B). Compared with AAm solutions (response surface shown in Figure 3E), zwitterionic formulations (Fig. 3D) exhibited a markedly faster gelation rate in both the initiation (50% faster than AAm, on average) and maturation of gelation (17% faster), represented by the time of G′ reaching 1 Pa at the early stage and to more than 90 % of the final plateau G′, respectively.

Using the results from DOE, we demonstrated the 3D printing of Z-gels with complex 3D structures, using projection SLA (Fig. 1A). Based on the composition and their corresponding gel time, Γ varied from 135 to 675 mJ cm^{-2} per layer in the desktop SLA (Autodesk Ember) printer, which corresponds to 6 to 30 s of exposure. These photoirradiation dosages are comparable with previous research using 2,4,6-trimethylbenzoyl-diphenylphosphine oxide (TPO) nanoparticles as a water dispersible photoinitiator, which required complicated modifications of TPO to overcome its insolubility in aqueous solutions [45]. Therefore, the riboflavin and TEOHA initiation chemistry we used is advantageous due to its simplicity, better water solubility, and great biocompatibility [36].

To demonstrate the capability of our SLA compatible Z-gels, we selected one zwitterionic solution (C_{reins}=4.37 M) with medium crosslink density (C_{MBA}=1.5 mol%) to print soft octopus arms. The 3D fabrication of this hydrogel was performed at a rate of 14 s (Γ~315 mJ cm^{-2}) per layer at a high resolution (50 μm thickness each layer) (Fig. 1C). A demonstration of high-resolution SLA (represented by a rose) is shown in a supporting video (Supplementary video 1).

Z-gel photopolymerization kinetics

We also observed a different gelation pattern of Z-gels compared to PAAm gels. The gelation rate of AAm resins relies more on the crosslink density represented by its steeper slope along the axis of C_{MBA}, compared with that of C_{resin} (Fig. 3E). The zwitterionic formulations, in which C_{resin} has an effect on the strength of ionic interactions, exhibit a stronger response to variations in C_{resin} on the response surface than that of C_{MBA} (Fig. 3D). This distinction clearly indicates that zwitterionic comonomer is critical to the fast gelation behavior of Z-gels (Fig. 2A). This finding is especially important as methacrylate groups of the MEDSAH are theoretically considered less reactive during the polymerization than the acrylate groups of AAm, owing to the higher stability of the tertiary radicals formed on MEDSAH than the secondary radicals formed on AAm. MEDSAH, however, is ionized and negatively charged in the aqueous solution over a large pH range (2< pH <10). Therefore, in the pre-gel solutions, zwitterions are assumed to present as acidic counter-ions to the basic TEOHA [44, 46]. As a result, the initiation in the Z-gel formulations might start from the zwitterions that are ionically interacting with TEOHA.

We tested this assumption on initiation by comparing the photo-DSC patterns of zwitterionic and AAm formulations. The zwitterionic solution showed two distinct but much narrower heat flow peaks, indicating a more rapid polymerization and a preference for certain

monomer. The AAm solution, however, showed only a broader single peak that indicates a slower polymerization (Fig. S5). Moreover, it was previously proposed that stronger ionic interactions, like those found in the zwitterionic formulations, cause the growing polymer chains to coil more so that the pendant acrylates are more easily and advantageously exposed to other free radical species [47].

We further characterized the Z-gel by a 400 MHz ^{1}H NMR spectra which showed the copolymerization of AAm and MEDSAH (Fig. S6). Thermal analyses were performed on both as prepared and freeze-dried hydrogels. DSC measurement of the dried Z-gel (Fig. S7A) indicated that the photopolymerized network behaves like a random copolymer with only one glass transition at ~140 °C. On the other hand, DSC of as prepared Z-gel showed a transition at ~150 °C, which was previously reported as the dehydration temperature [48] (Fig. 4A). Interestingly, the dehydration temperature of counterpart PAAm hydrogel was ~120 °C. We attribute this 30 °C difference to greater hydrophilicity of the Z-gels, which leads to stronger water affinity.

From TGA, the as prepared Z-gel was more thermally stable than PAAm hydrogel by presenting smaller weight loss before 200 °C, probably owing to the additional ionic crosslinks (Fig. 4B). Dried Z-gel represented similar behavior with the onset degradation temperature at ~250 °C, which is about 30 °C higher than that of dried PAAm (Fig. S7B).

Antifouling tests

We compare the antifouling performance of the zwitterionic and PAAm hydrogels based on a protein absorption measurement using bovine serum albumin (BSA) as the model protein. After six hours soaking in the BSA solution, the Z-gels absorbed significantly less (58.2 %) BSA

than the counterpart PAAm hydrogels (81.2 μg mL^{-1} BSA absorption of PAAm hydrogels versus 33.5 μg mL^{-1} of the corresponding Z-gels). This behavior agrees with previously reported research which applied zwitterionic polymers [49-51]. We attribute the significantly improved antifouling behavior to the super hydrophilicity of the zwitterionic moieties, which absorb excessive layers of water molecules on the hydrogel surface and thus exhibit strong repulsive forces against surrounding protein molecules (Fig. 1D) [49]. The antifouling performance is believed to be positively correlated to the surface density of the zwitterionic groups [52].

Conclusions

3D printing via projection stereolithography is a promising approach for the construction of complex soft material systems for future applications in smart materials, soft actuators and sensors, and biomedical devices. The limited availability of hydrogel materials, however, restricts progress in many of these areas. In this paper, we report and characterize a novel SLA platform that integrates zwitterionic chemistry and a simple but efficient aqueous photoinitiation system. The introduction of the zwitterionic comonomer into acrylamide has significantly improved the patterning rate of the SLA system and overcome the weakness of the traditional DN hydrogels, thereby enabling rapid fabrication of elastic and tough hydrogels. Furthermore, we employed DOE methodology to perform a systematic optimization and investigation of gelation rate, swelling behavior, and mechanical properties and used the results to guide the hydrogel formulations for optimal properties.

We found that the copolymerization of MEDSAH and AAm, using the biocompatible photochemistry of riboflavin and TEOHA, produced hybrid hydrogels with significantly improved antifouling properties, which could make these materials well suited for 3D printed biomedical devices. Further, our platform is versatile and can be easily modified for specific applications and desirable properties. For example, instead of using AAm, thermally responsive hydrogel materials such as *N*-isopropylacrylamide could be used as implantable and targeted drug delivery devices to broaden the intended application space of these materials.

Acknowledgements

This work is supported by Air Force Office of Scientific Research, Contract: FA9550-18-1-0243. We also acknowledge use of the Cornell Center for Materials Research Shared Facilities which are supported through the NSF MRSEC program (DMR-1719875).

Conflict of Interest

The authors declare no conflict of interest.

References

[1] Lee KY, Mooney DJ. Hydrogels for tissue engineering. Chemical reviews. 2001;101:1869-80.
[2] Hoffman AS. Hydrogels for biomedical applications. Advanced drug delivery reviews. 2002;54:3-12.
[3] Matsusaki M, Yoshida H, Akashi M. The construction of 3D-engineered tissues composed of cells and extracellular matrices by hydrogel template approach. Biomaterials. 2007;28:2729-37.
[4] Melchels FP, Feijen J, Grijpma DW. A review on stereolithography and its applications in biomedical engineering. Biomaterials. 2010;31:6121-30.
[5] Willner I. Stimuli-Controlled Hydrogels and Their Applications. ACS Publications; 2017.
[6] Maruo S, Ikuta K. Submicron stereolithography for the production of freely movable mechanisms by using single-photon polymerization. Sensors and Actuators A: Physical. 2002;100:70-6.
[7] Tumbleston JR, Shirvanyants D, Ermoshkin N, Janusziewicz R, Johnson AR, Kelly D, et al. Continuous liquid interface production of 3D objects. Science. 2015;347:1349-52.
[8] Chartier T, Ferrato M, Baumard J. Debinding of ceramics: a review. Ceramicaacta. 1994;6:17-27.
[9] Chartier T, Hinczewski C, Corbel S. UV curable systems for tape casting. Journal of the European Ceramic Society. 1999;19:67-74.
[10] Dulieu-Barton J, Fulton M. Mechanical properties of a typical stereolithography resin. Strain. 2000;36:81-7.
[11] Drury JL, Mooney DJ. Hydrogels for tissue engineering: scaffold design variables and applications. Biomaterials. 2003;24:4337-51.
[12] White EM, Yatvin J, Grubbs JB, Bilbrey JA, Locklin J. Advances in smart materials: Stimuli-responsive hydrogel thin films. Journal of Polymer Science Part B: Polymer Physics. 2013;51:1084-99.
[13] Gong JP. Why are double network hydrogels so tough? Soft Matter. 2010;6:2583-90.
[14] Gong JP, Katsuyama Y, Kurokawa T, Osada Y. Double-network hydrogels with extremely high mechanical strength. Advanced Materials. 2003;15:1155-8.
[15] Sun J-Y, Zhao X, Illeperuma WR, Chaudhuri O, Oh KH, Mooney DJ, et al. Highly stretchable and tough hydrogels. Nature. 2012;489:133-6.
[16] Yuk H, Zhang T, Lin S, Parada GA, Zhao X. Tough bonding of hydrogels to diverse non-porous surfaces. Nature materials. 2016;15:190-6.
[17] Zhao X. Multi-scale multi-mechanism design of tough hydrogels: building dissipation into stretchy networks. Soft Matter. 2014;10:672-87.
[18] Odent J, Wallin TJ, Pan W, Kruemplestaedter K, Shepherd RF, Giannelis EP. Highly Elastic, Transparent, and Conductive 3D-Printed Ionic Composite Hydrogels. Advanced Functional Materials. 2017.
[19] Bakarich SE, Pidcock GC, Balding P, Stevens L, Calvert P. Recovery from applied strain in interpenetrating polymer network hydrogels with ionic and covalent cross-links. Soft Matter. 2012;8:9985-8.
[20] Bakarich SE, Beirne S, Wallace GG, Spinks GM. Extrusion printing of ionic–covalent entanglement hydrogels with high toughness. Journal of Materials Chemistry B. 2013;1:4939-46.
[21] Peak CW, Wilker JJ, Schmidt G. A review on tough and sticky hydrogels. Colloid and Polymer Science. 2013;291:2031-47.

[22] Hoffman AS. Hydrogels for biomedical applications. Advanced drug delivery reviews. 2012;64:18-23.
[23] Yang CH, Wang MX, Haider H, Yang JH, Sun J-Y, Chen YM, et al. Strengthening alginate/polyacrylamide hydrogels using various multivalent cations. ACS applied materials & interfaces. 2013;5:10418-22.
[24] Şolpan D, Torun M, Güven O. The usability of (sodium alginate/acrylamide) semi-interpenetrating polymer networks on removal of some textile dyes. J Appl Polym Sci. 2008;108:3787-95.
[25] Kamata H, Akagi Y, Kayasuga-Kariya Y, Chung U-i, Sakai T. "Nonswellable" hydrogel without mechanical hysteresis. Science. 2014;343:873-5.
[26] Bertolotti S, Previtali C, Rufs A, Encinas M. Riboflavin/triethanolamine as photoinitiator system of vinyl polymerization. A mechanistic study by laser flash photolysis. Macromolecules. 1999;32:2920-4.
[27] Orellana B, Rufs A, Encinas M, Previtali C, Bertolotti S. The photoinitiation mechanism of vinyl polymerization by riboflavin/triethanolamine in aqueous medium. Macromolecules. 1999;32:6570-3.
[28] Cheng G, Li G, Xue H, Chen S, Bryers JD, Jiang S. Zwitterionic carboxybetaine polymer surfaces and their resistance to long-term biofilm formation. Biomaterials. 2009;30:5234-40.
[29] Tanaka M, Sato K, Kitakami E, Kobayashi S, Hoshiba T, Fukushima K. Design of biocompatible and biodegradable polymers based on intermediate water concept. Polymer Journal. 2015;47:114-21.
[30] Bernards MT, Cheng G, Zhang Z, Chen S, Jiang S. Nonfouling polymer brushes via surface-initiated, two-component atom transfer radical polymerization. Macromolecules. 2008;41:4216-9.
[31] Nandivada H, Villa-Diaz LG, O'Shea KS, Smith GD, Krebsbach PH, Lahann J. Fabrication of synthetic polymer coatings and their use in feeder-free culture of human embryonic stem cells. Nature protocols. 2011;6:1037-43.
[32] Osaheni AO, Finkelstein EB, Mather PT, Blum MM. Synthesis and characterization of a zwitterionic hydrogel blend with low coefficient of friction. Acta Biomaterialia. 2016.
[33] Zhang L, Cao Z, Bai T, Carr L, Ella-Menye JR, Irvin C, et al. Zwitterionic hydrogels implanted in mice resist the foreign-body reaction. Nature biotechnology. 2013;31:553-6.
[34] Zhang Z, Chao T, Liu L, Cheng G, Ratner BD, Jiang S. Zwitterionic hydrogels: an in vivo implantation study. Journal of Biomaterials Science, Polymer Edition. 2009;20:1845-59.
[35] Yin H, Akasaki T, Sun TL, Nakajima T, Kurokawa T, Nonoyama T, et al. Double network hydrogels from polyzwitterions: high mechanical strength and excellent anti-biofouling properties. Journal of Materials Chemistry B. 2013;1:3685-93.
[36] Nguyen AK, Gittard SD, Koroleva A, Schlie S, Gaidukeviciute A, Chichkov BN, et al. Two-photon polymerization of polyethylene glycol diacrylate scaffolds with riboflavin and triethanolamine used as a water-soluble photoinitiator. Regenerative medicine. 2013;8:725-38.
[37] Schmid AJ, Schroeder R, Eckert T, Radulescu A, Pich A, Richtering W. Synthesis and solution behaviour of stimuli-sensitive zwitterionic microgels. Colloid and Polymer Science. 2015;293:3305-18.
[38] Das M, Sanson N, Kumacheva E. Zwitterionic poly (betaine-n-isopropylacrylamide) microgels: properties and applications. Chemistry of Materials. 2008;20:7157-63.

[39] Zhang M, Shan C, Liu L, Liao J, Chen Q, Zhu M, et al. Facilitating anion transport in polyolefin-based anion exchange membranes via bulky side chains. ACS applied materials & interfaces. 2016;8:23321-30.
[40] Varley R. Ionomers as self healing polymers. Self Healing Materials: Springer; 2007. p. 95-114.
[41] Guo J, Long R, Mayumi K, Hui C-Y. Mechanics of a Dual Cross-Link Gel with Dynamic Bonds: Steady State Kinetics and Large Deformation Effects. Macromolecules. 2016;49:3497-507.
[42] Long R, Mayumi K, Creton C, Narita T, Hui C-Y. Rheology of a dual crosslink self-healing gel: Theory and measurement using parallel-plate torsional rheometry. Journal of Rheology (1978-present). 2015;59:643-65.
[43] Kuo CK, Ma PX. Ionically crosslinked alginate hydrogels as scaffolds for tissue engineering: Part 1. Structure, gelation rate and mechanical properties. Biomaterials. 2001;22:511-21.
[44] Encinas M, Rufs A, Bertolotti S, Previtali C. Free radical polymerization photoinitiated by riboflavin/amines. Effect of the amine structure. Macromolecules. 2001;34:2845-7.
[45] Pawar AA, Saada G, Cooperstein I, Larush L, Jackman JA, Tabaei SR, et al. High-performance 3D printing of hydrogels by water-dispersible photoinitiator nanoparticles. Science advances. 2016;2:e1501381.
[46] Wu L, Jasinski J, Krishnan S. Carboxybetaine, sulfobetaine, and cationic block copolymer coatings: a comparison of the surface properties and antibiofouling behavior. J Appl Polym Sci. 2012;124:2154-70.
[47] Haraguchi K, Li H-J, Matsuda K, Takehisa T, Elliott E. Mechanism of forming organic/inorganic network structures during in-situ free-radical polymerization in PNIPA-clay nanocomposite hydrogels. Macromolecules. 2005;38:3482-90.
[48] Lalani R, Liu L. Synthesis, characterization, and electrospinning of zwitterionic poly (sulfobetaine methacrylate). Polymer. 2011;52:5344-54.
[49] Zhao Y-F, Zhu L-P, Yi Z, Zhu B-K, Xu Y-Y. Zwitterionic hydrogel thin films as antifouling surface layers of polyethersulfone ultrafiltration membranes anchored via reactive copolymer additive. Journal of Membrane Science. 2014;470:148-58.
[50] Xiang T, Luo C-D, Wang R, Han Z-Y, Sun S-D, Zhao C-S. Ionic-strength-sensitive polyethersulfone membrane with improved anti-fouling property modified by zwitterionic polymer via in situ cross-linked polymerization. Journal of Membrane Science. 2015;476:234-42.
[51] Razi F, Sawada I, Ohmukai Y, Maruyama T, Matsuyama H. The improvement of antibiofouling efficiency of polyethersulfone membrane by functionalization with zwitterionic monomers. Journal of membrane science. 2012;401:292-9.
[52] Ma C, Zhou H, Wu B, Zhang G. Preparation of polyurethane with zwitterionic side chains and their protein resistance. ACS applied materials & interfaces. 2011;3:455-61.

A

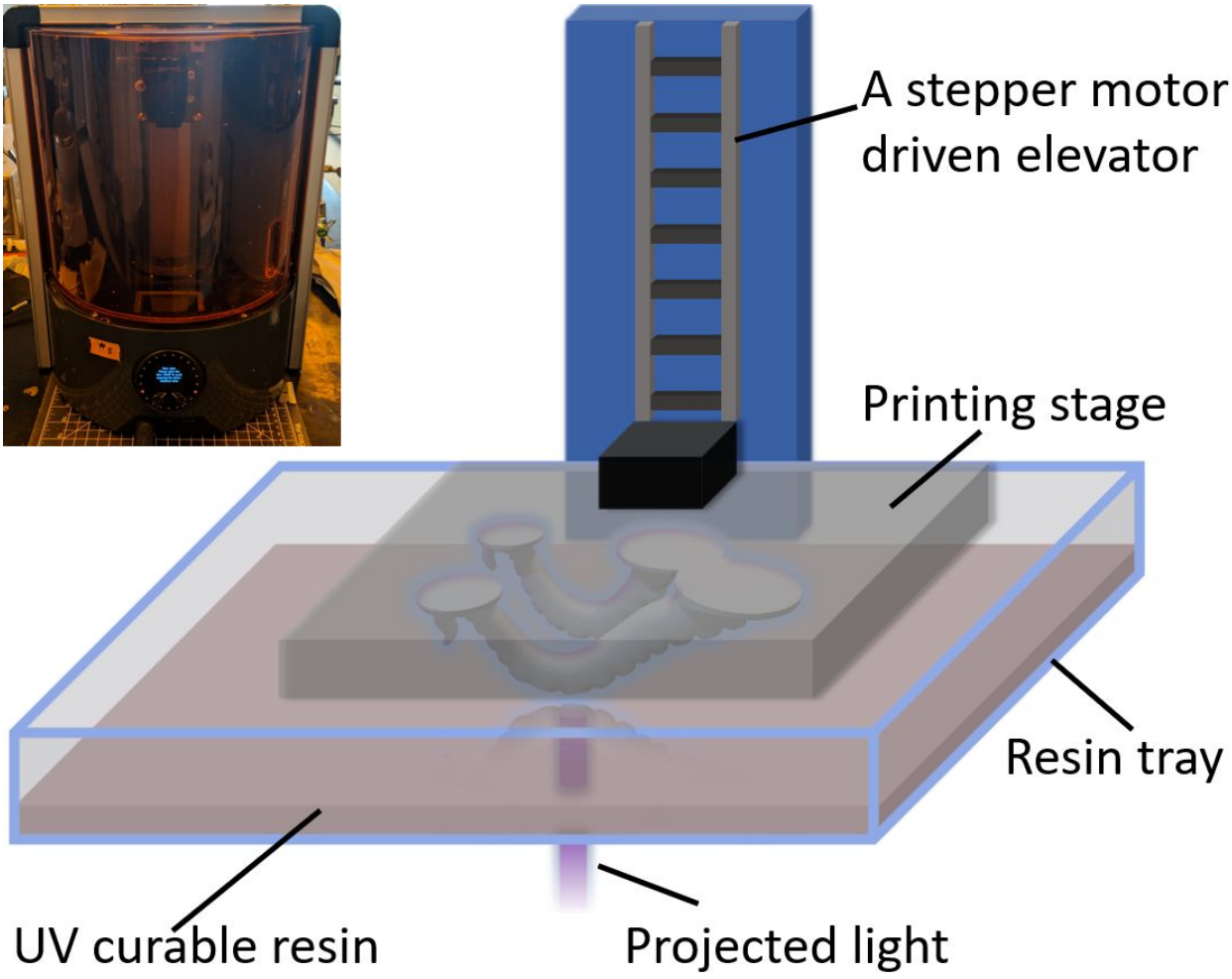
A stepper motor driven elevator
Printing stage
Resin tray
UV curable resin
Projected light

B

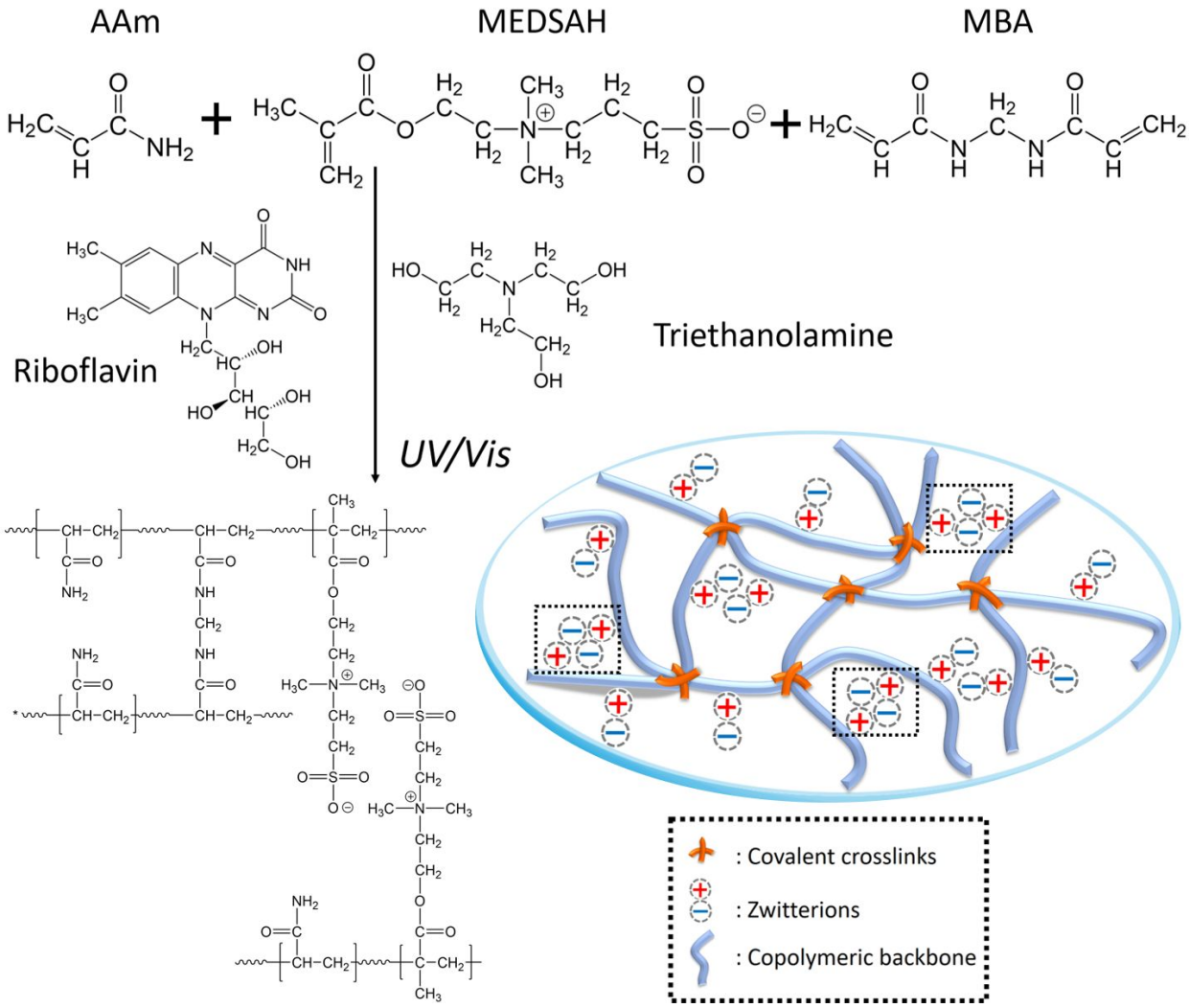
AAm
MEDSAH
MBA
Riboflavin
Triethanolamine
UV/Vis
: Covalent crosslinks
: Zwitterions
: Copolymeric backbone

C

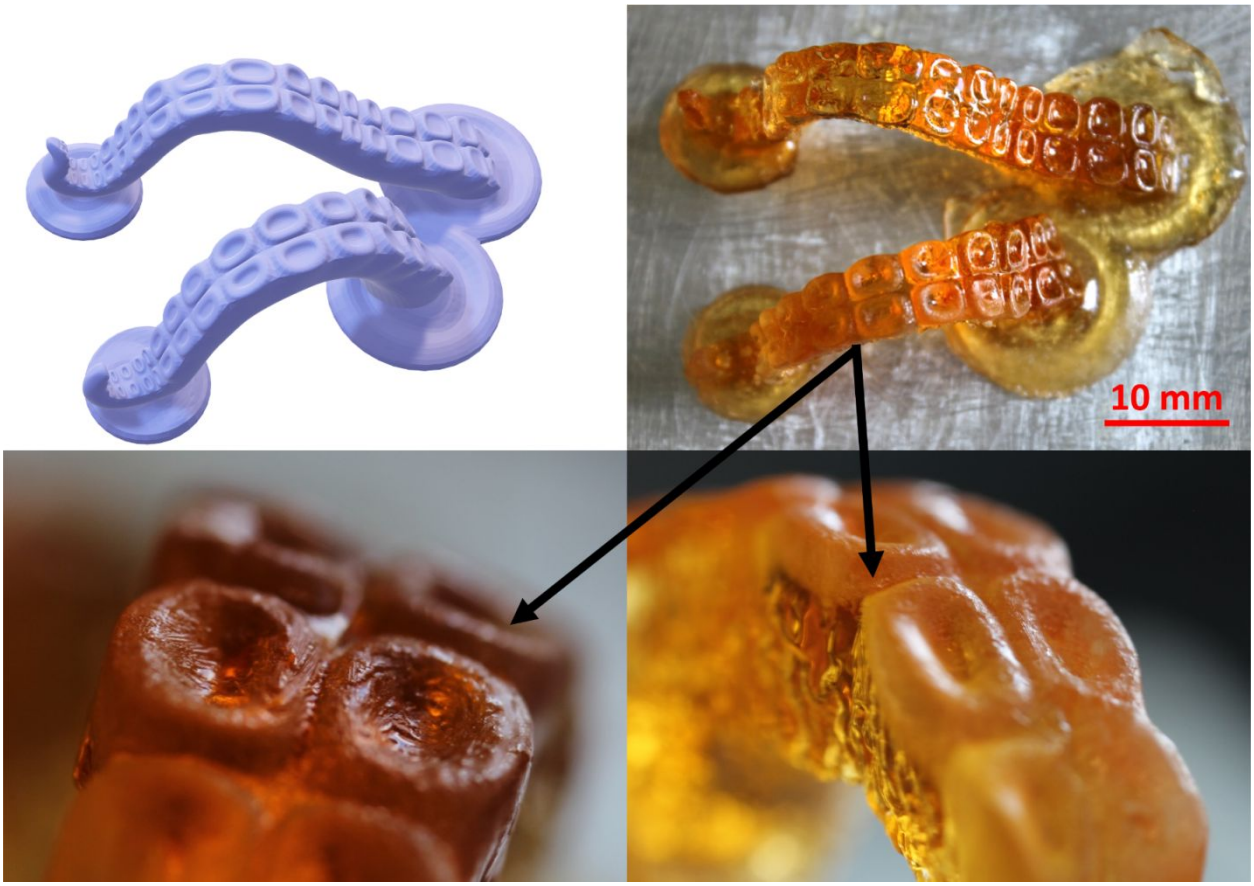

D

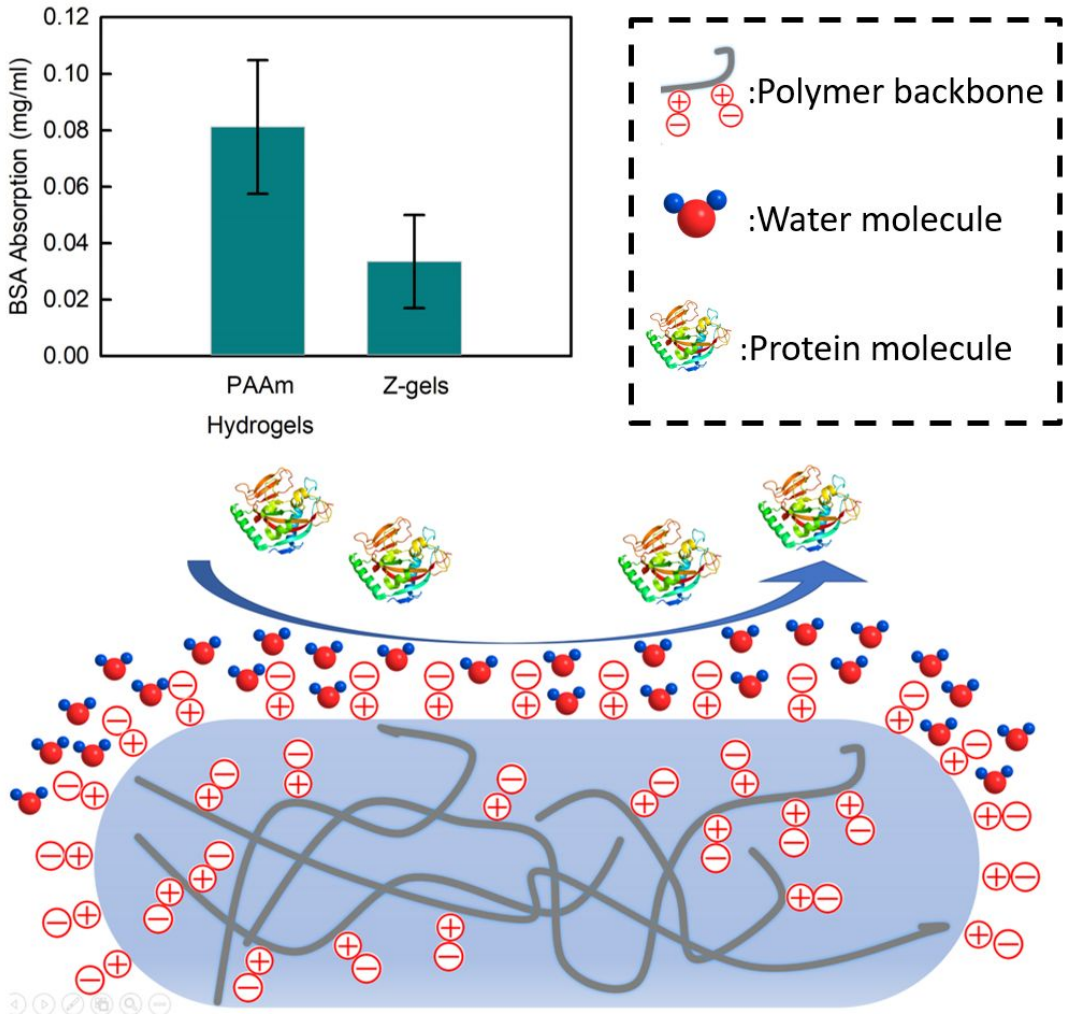

Figure 1 Fabrication of antifouling Z-gels through optical stereolithography: A. Schematic representation of the projection-stereolithography. **B.** Zwitterionic hybrid hydrogel fabricated with acrylamide (AAm) and [2-(methacryloyloxy)ethyl]dimethyl-(3-sulfopropyl)ammonium hydroxide (MEDSAH), having ionic crosslinks among the zwitterionic moieties and chemically crosslinked by MBA; riboflavin as the photoinitiator, and triethanolamine as the coinitiator. **C.** Fast fabrication of octopus arms with 50μm resolution, at the speed of 14 s per layer, through SLA. **D**, Comparison of BSA absorption of PAAm and the counterpart Z-gel with the same crosslink density. Lower figure shows the mechanism of improved antifouling property by using zwitterionic chemistry in the hydrogel resin.

A

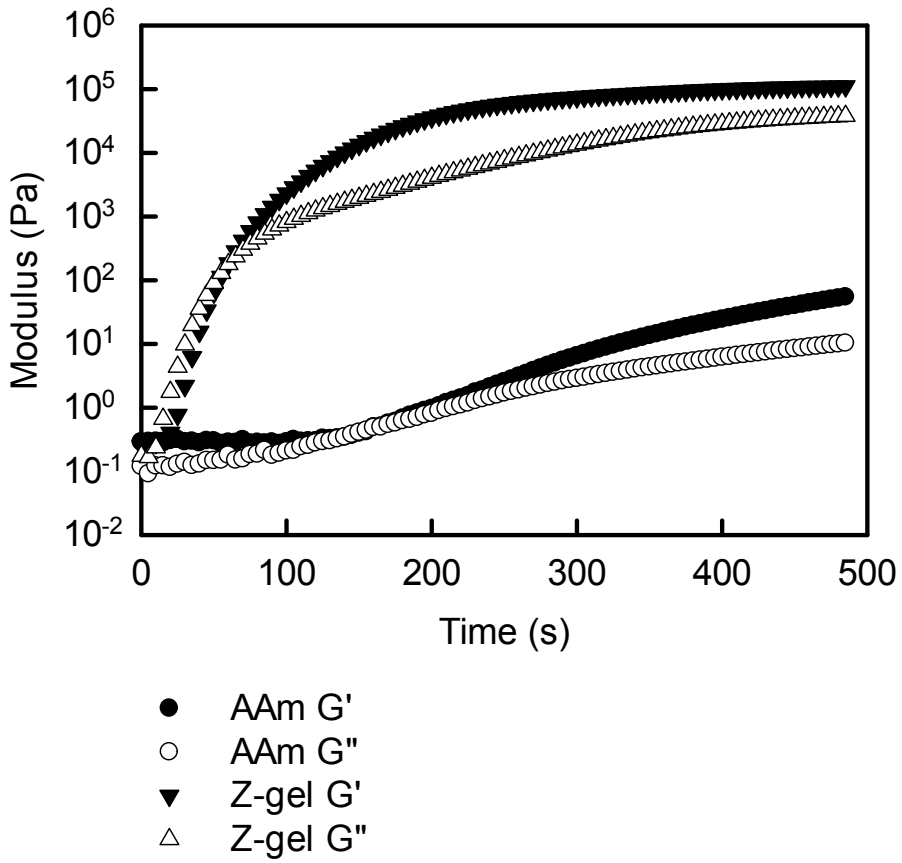
Modulus (Pa)
10^6
10^5
10^4
10^3
10^2
10^1
10^0
10^{-1}
10^{-2}
0
100
200
300
400
500
Time (s)
AAm G'
AAm G"
Z-gel G'
Z-gel G"

B

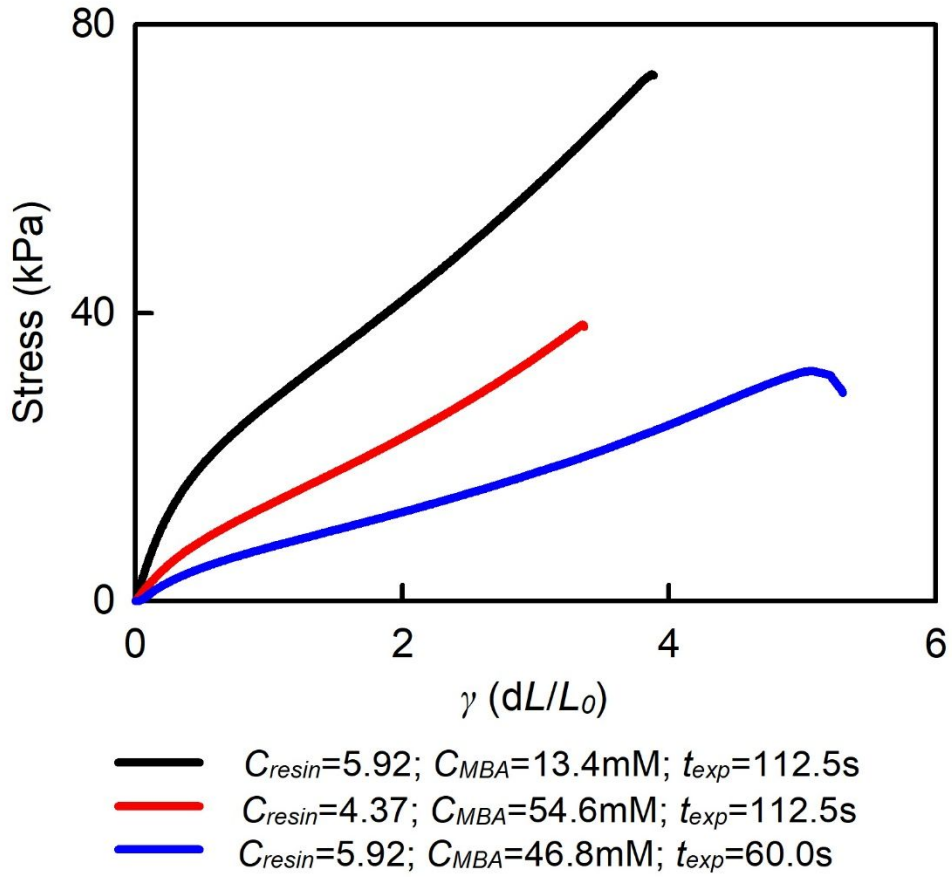
80
40
0
Stress (kPa)
0
2
4
6
γ (dL/L0)
Cresin=5.92; CMBA=13.4mM; texp=112.5s
Cresin=4.37; CMBA=54.6mM; texp=112.5s
Cresin=5.92; CMBA=46.8mM; texp=60.0s

C

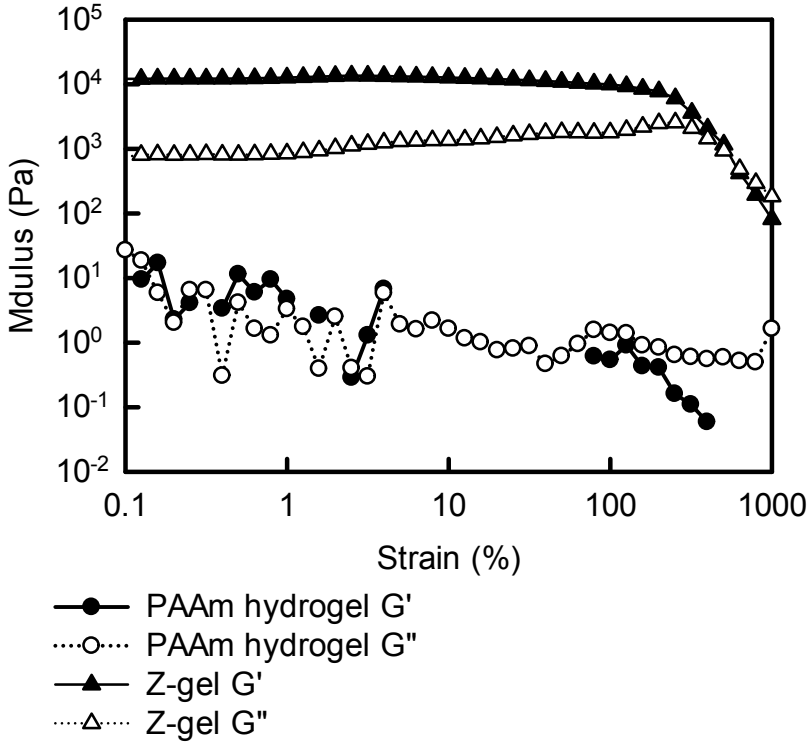
Mdulus (Pa)
10^5
10^4
10^3
10^2
10^1
10^0
10^{-1}
10^{-2}
0.1
1
10
100
1000
Strain (%)
PAAm hydrogel G'
PAAm hydrogel G"
Z-gel G'
Z-gel G"

D

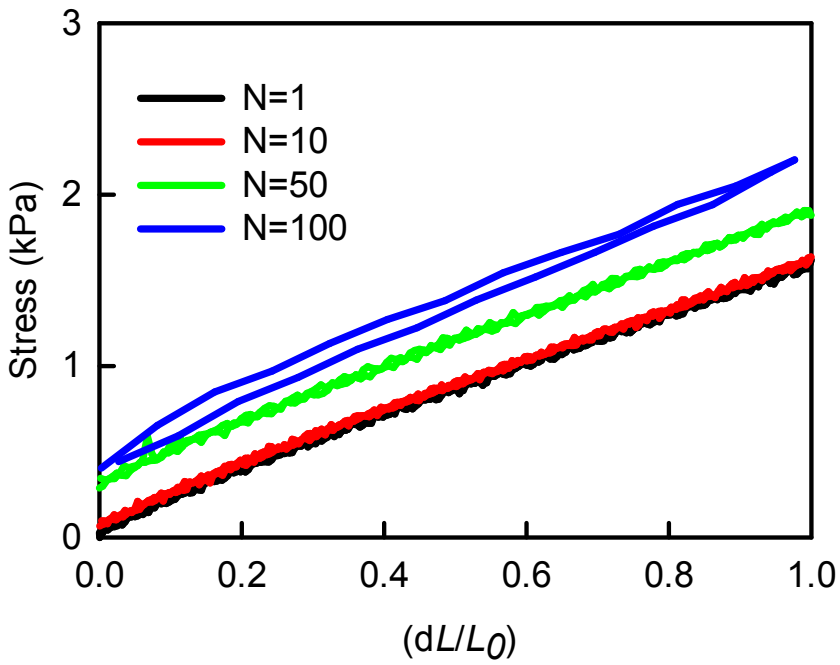

E

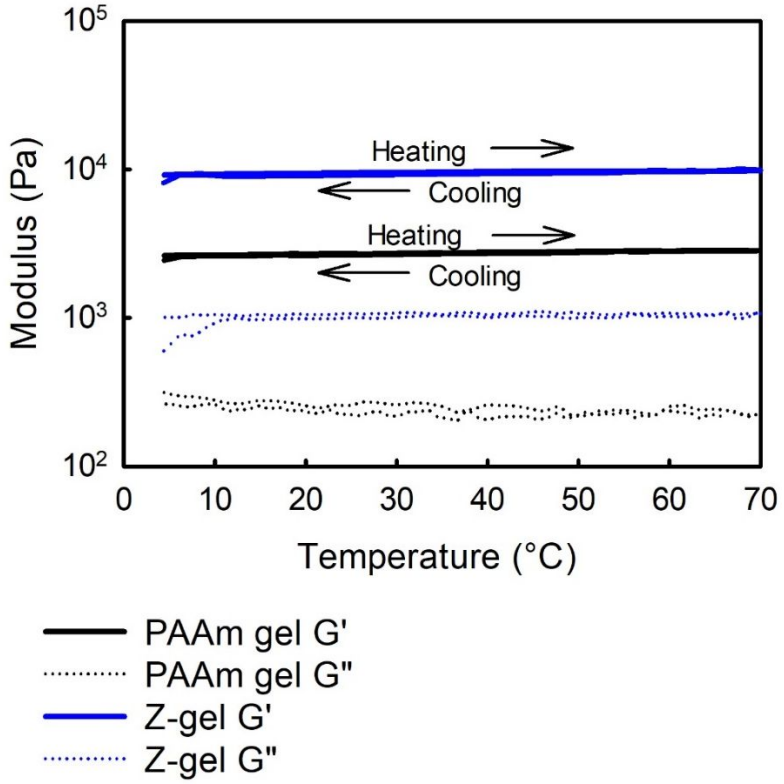

Figure 2 Mechanical properties of the Z-gel. A. The measurements of G', G" of the Z-gel during the photopolymerization, in comparison to the molar equivalent AAm hydrogels, respectively. **B**. Ultimate strain (γ) of the Z-gels with different monomer content (C_{resin}), crosslink density (C_{MBA}) and photoirradiation dosages (represented by t_{exp} under Omnicure 1500). **C.** Significant improvement in stiffness of the Z-gel over PAAm hydrogel has been observed in typical strain sweep rheological tests. Both Z-gel and PAAm hydrogels used in this measurement have equivalent resin composition (C_{resin}=4.374, C_{MBA}=1.5 mol%) and were exposed for same amount of time (t_{exp} =112.5 s). **D.** Cyclic tensile tests of the Z-gel for 100 cycles. The dog bone shaped Z-gel was stretched to tensile strain (γ =1) at the speed of 0.1 per min. **E.** The heating-cooling cycle of temperature sweep rheological tests of as prepared PAAm hydrogel and Z-gels. Both Z-gel and PAAm hydrogels (same crosslink density) were cast in PDMS mold and exposed under Omnicure 1500 until cured.

A

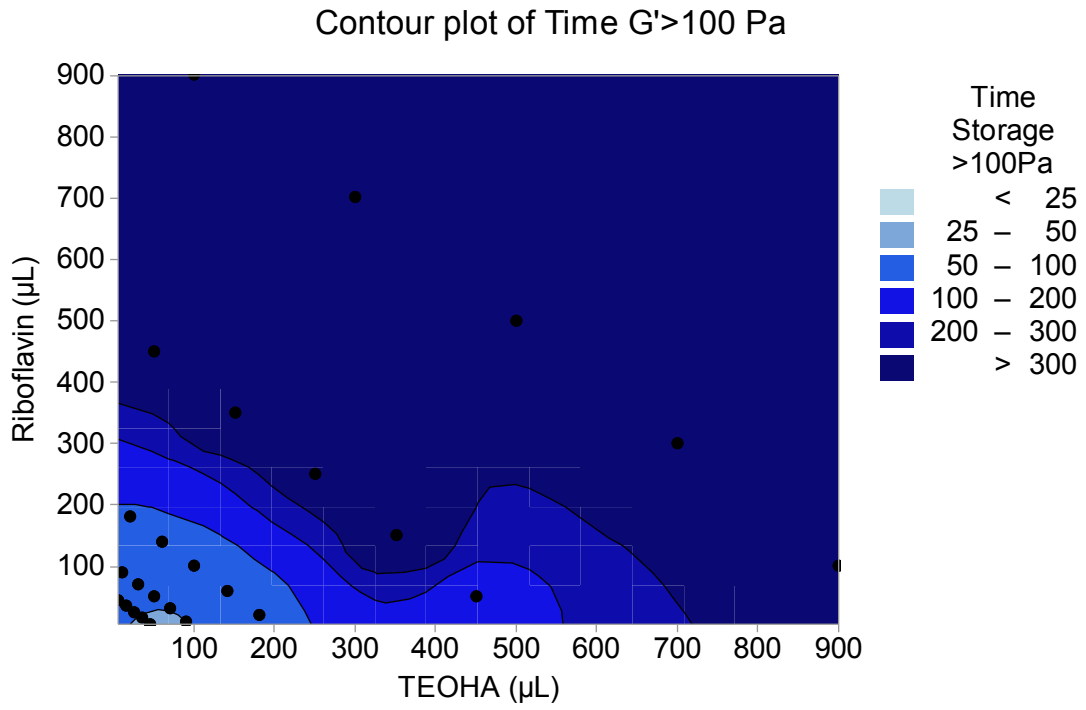
Contour plot of Time G'>100 Pa
Riboflavin (µL)
TEOHA (µL)
Time Storage >100Pa
< 25
25 – 50
50 – 100
100 – 200
200 – 300
> 300

B

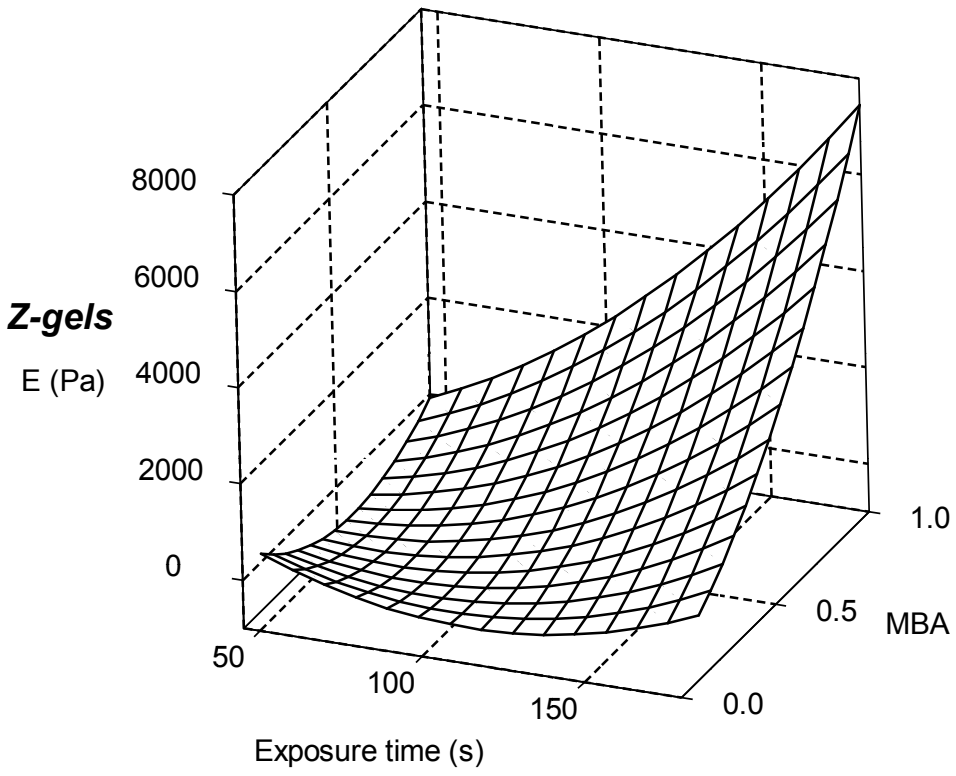
Z-gels
E (Pa)
Exposure time (s)
MBA

C

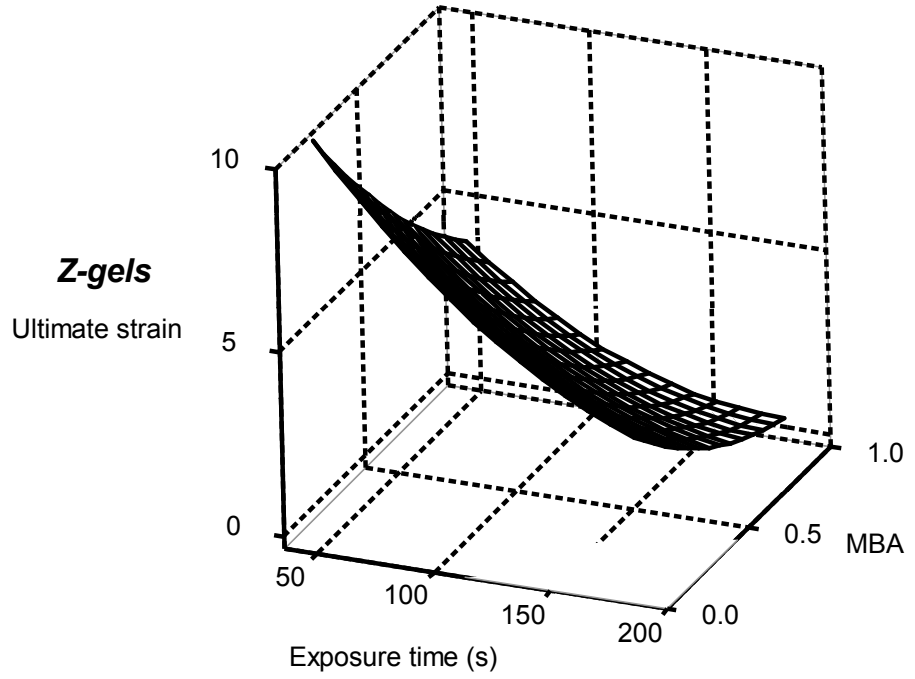
Z-gels
Ultimate strain
10
5
0
50
100
150
200
Exposure time (s)
0.0
0.5
1.0
MBA

D

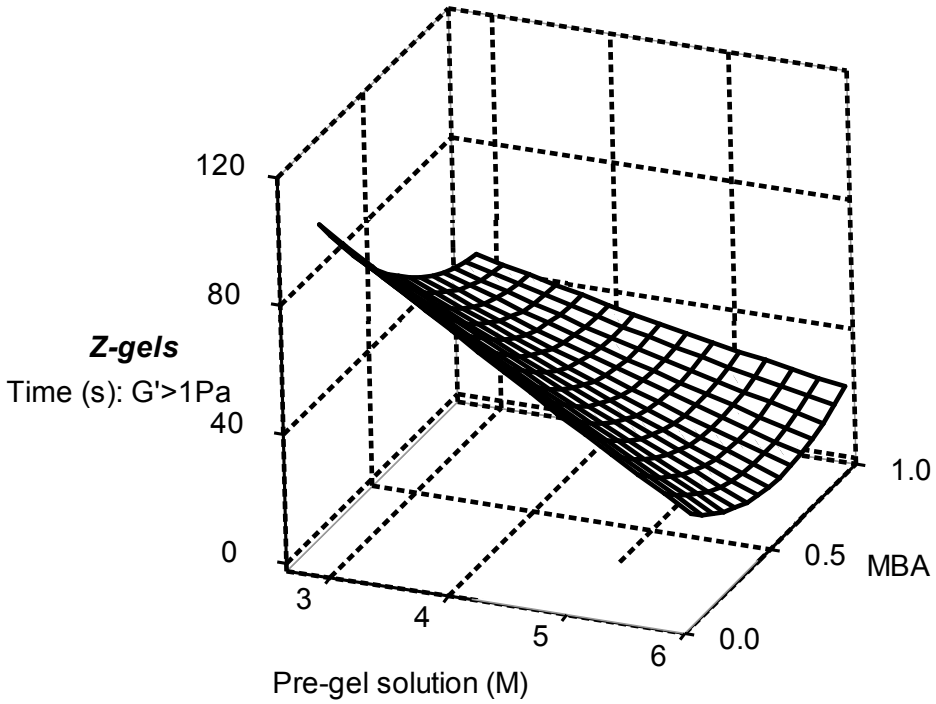
Z-gels
Time (s): G'>1Pa
120
80
40
0
3
4
5
6
Pre-gel solution (M)
0.0
0.5
1.0
MBA

E

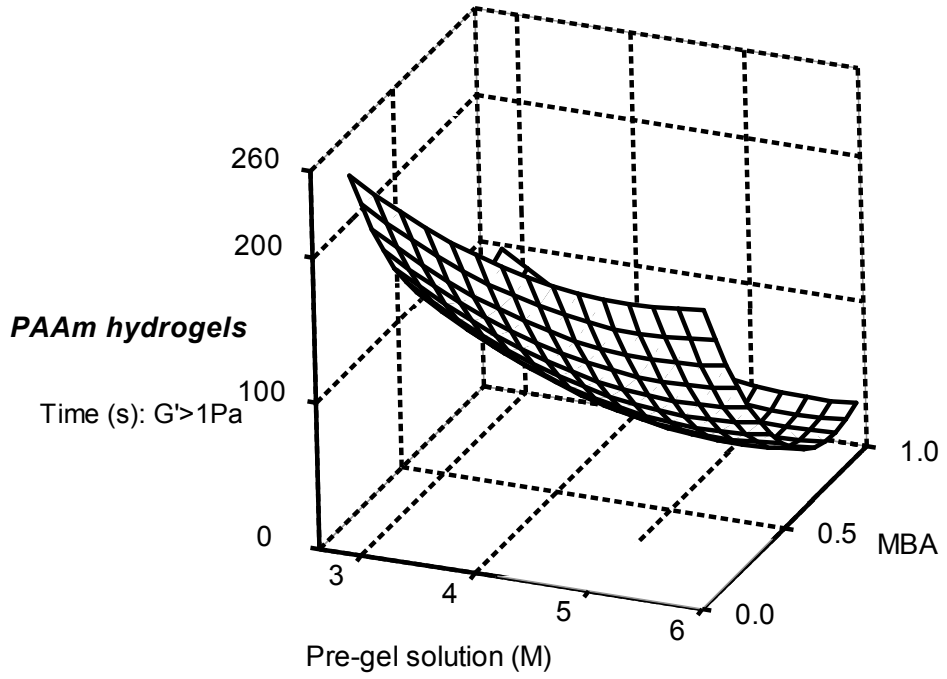

Figure 3 Investigation and modeling of the Z-gel system. A. The contour map of time when G'>100 Pa vs. riboflavin and TEOHA ratio, based on the mixture design. Lighter colors indicate faster gellation. **B.** The response surface plot of elastic modulus *E* (kPa) against the monomer content and exposure time. The contents of MBA as chemical crosslinker in DOE models were represented by their relative ratio to monomer contents (The value 1 equals to 1/42 mol of monomer content, which was predetermined as the upper limit for MBA). **C.** The response surface plot of the ultimate strain γ_{ult} against the MBA content and exposure time based on Box-Behnken design. **D**. The response surface plot of time when G'>1Pa for Z-gels. **E**. The response surface plot of time when G'>1Pa for PAAm hydrogels, which are more dependent on the crosslink density, compared with the monomer content.

A

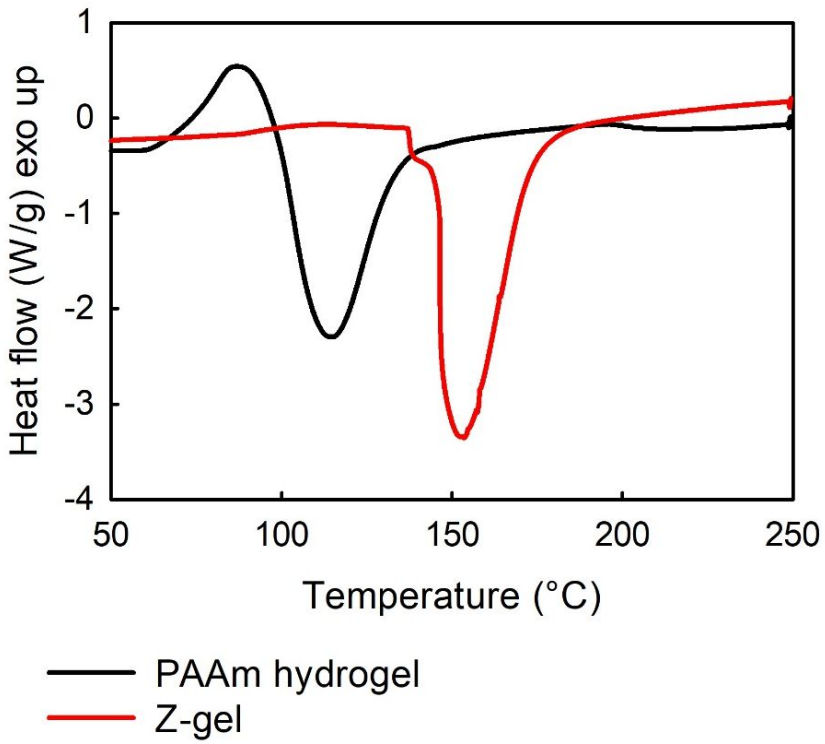
Heat flow (W/g) exo up
1
0
-1
-2
-3
-4
50
100
150
200
250
Temperature (°C)
PAAm hydrogel
Z-gel

B

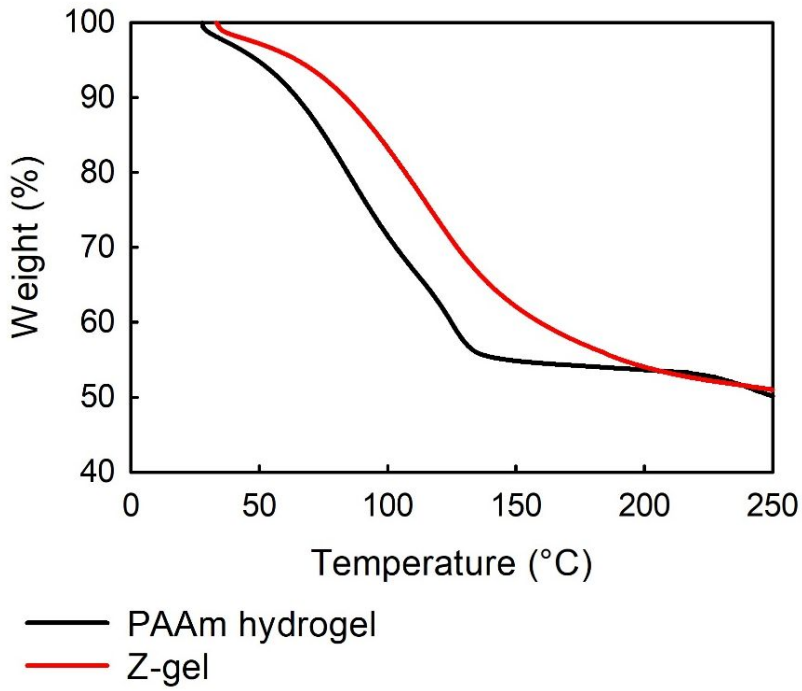

Figure 4 Thermal properties of the as prepared Z-gel and PAAm hydrogel. A. DSC measurement of as prepared Z-gel and counterpart PAAm hydrogel. **B**. TGA of as prepared Z-gel and PAAm hydrogel.

Table 1. The combinations of riboflavin and TEOHA contents (based on mixture design), and their effects on the gelation speed of PAAm hydrogels (based on the photo-rheological measurements). Sampling interval was 0.5 s. The pre-gel solutions of AAm contained 5.9 M AAm and ~2.4 mol% MBA.

Standard order	Riboflavin (μL)	Triethanolamine (μL)	When G'>1 Pa	When G'>10 Pa	When G'>10^2 Pa	When G'>10^3 Pa	When G'>10^4 Pa
1	45	5	24	39.5	72	112	165
2	5	45	17.5	25	37	105	116.5
3	25	25	19	29	46.5	66.5	132.5
4	35	15	22	35	60	89	131.5
5	15	35	18.5	27.5	39	55	91
6	90	10	23.5	34.5	65.5	113.5	166.5
7	10	90	18.5	26.5	38.5	53.5	83.5
8	50	50	22	32.5	52	76	113.5
9	70	30	20.5	30.5	58.5	102.5	158
10	30	70	18.5	27	42.5	64.5	127.5
11	180	20	26	38.5	96.5	198.5	1000
12	20	180	20	28.5	41.5	54	78
13	100	100	22	31.5	61	91.5	139
14	140	60	35	48	77	116	188
15	60	140	34	48.5	70.5	92	129
16	450	50	1000*	1000	1000	1000	1000
17	50	450	60	78.5	108.5	150	222
18	250	250	1000	1000	1000	1000	1000
19	350	150	1000	1000	1000	1000	1000
20	150	350	211	272	1000	1000	1000
21	900	100	1000	1000	1000	1000	1000
22	100	900	1000	1000	1000	1000	1000
23	500	500	1000	1000	1000	1000	1000
24	700	300	1000	1000	1000	1000	1000
25	300	700	1000	1000	1000	1000	1000

* The gelation time was assigned as 1000 s when the hydrogel failed to reach certain level of G′ during the photo-rheological tests which last for 500 s.

Table 2. Box-Behnken design of a 3-factor (C_{resin}, C_{MBA} and t_{exp}) experiments and the corresponding responses (G′, G″, ultimate strain, Young's modulus and swelling ratio). The as prepared Z-gels were subjected to strain sweep rheological tests (G′ and G″, data were taken when the strain was 10% at the fixed angular frequency at 1 rad/s).

Standard order	t_{exp} (s)	C_{MBA}*	C_{resin} (M)	G' (Pa)	G" (Pa)	Ultimate strain (%)	Young's modulus (kPa)	Swelling ratio q
1	45	0.1	4.374	280	335	1000.0**	1**	10**
2	180	0.1	4.374	2610	1590	357.9	228	3.96
3	45	1	4.374	14800	3610	381.8	17	1.48
4	180	1	4.374	989	2250	67.2	7599	1.68
5	45	0.55	2.824	1	1.15	1000.0	1	10
6	180	0.55	2.824	783	341	239.8	93	1.47
7	45	0.55	5.924	2670	850	368.3	51	2.03
8	180	0.55	5.924	3480	1390	53.8	7522	2.40
9	112.5	0.1	2.824	1	1.15	1000.0	1	10
10	112.5	1	2.824	879	224	164.0	26	1.19
11	112.5	0.1	5.924	15700	4690	328.0	611	3.29
12	112.5	1	5.924	116000	20200	36.0	6992	1.61
13	112.5	0.55	4.374	8940	1690	309.1	107	2.06
14	112.5	0.55	4.374	6250	914	309.1	107	1.96
15	112.5	0.55	4.374	9910	1790	309.1	107	2.02

*C_{MBA} as chemical crosslinker was represented by their relative ratio to C_{resin} (The value 1 equals to 1/42 mol of C_{resin}, which was predetermined as the upper limit for C_{MBA}).

**The ultimate strain (%), Young's modulus and swelling ratio were assigned as 1000.0 %, 1 kPa and 10, respectively, for hydrogels that were too soft to use in tensile tests.

Table 3. Central composite design (CCD) of 2-factor (C_{resin} and C_{MBA}) photo-rheological tests and the corresponding response (time when G′ >1 Pa) to represent the initiation of gelation. All samples were subjected to 500 s exposure from Omnicure 1500.

	C_{resin} (M)	C_{MBA}	Z-gel solutions When G′>1 Pa (s)	AAm solutions When G′>1 Pa (s)
1	2.824	0.1	102.5	239.0
2	5.924	0.1	26.5	198.0
3	2.824	1	46.0	88.5
4	5.924	1	19.0	33.5
5	2.824	0.55	59.0	129.5
6	5.924	0.55	19.5	43.5
7	4.374	0.1	66.0	201.5
8	4.374	1	33.5	44.0
9	4.374	0.55	36.0	56.5
10	4.374	0.55	36.0	56.5
11	4.374	0.55	36.0	56.5
12	4.374	0.55	36.0	56.5
13	4.374	0.55	36.0	56.5

* C_{MBA} was represented by their relative ratio to C_{resin} (The value 1 equals to 1/42 mol of C_{resin}, which was predetermined as the upper limit for MBA).